REFERENCES

1. C. M.Lampert, *Solar Energy Mater. Solar Cells*, **32**, 307 (1994) and references therein.
2. M. Chigane and M. Ishikawa, *This Journal*, **141**, 3449 (1994).
3. M. K. Capenter, R. S. Conel, and D. A. Corrigan, *Solar Energy Mater.*, **16**, 333 (1987).
4. J. S. E. M. Svensson and C. G. Granqvist, *ibid.*, **16**, 19 (1987).
5. K. Hinokuma, A. Kishimoto, and T. Kudo, *This Journal*, **141**, 876 (1994).
6. A. J. Bard, R. Parsons, and J. Joran, *Standard Potentials in Aqueous Solution*, IUPAC/Marcel Dekker, New York (1985).
7. A. Guerfi, R. W. Paynter, and L. H. Dao, *This Journal*, **142**, 3457 (1995).
8. H. Bode, K. Dehmelt, and J. Witte, *Electrochim. Acta*, **11**, 1079 (1966).
9. P. V. Kamath, M. Dixit, L. Indira, A. K. Shukla, V. G. Kumar, and N. Munichandraiah, *This Journal*, **141**, 2956 (1994).
10. M. Pourbaix, *Atlas of Electrochemical Eqilibria in Aqueous Solution*, NACE, Houston, TX (1974).
11. Z. Mao and R. E. White, *This Journal*, **139**, 1282 (1992).
12. P. Delichere, S. Joiret, A. H. Goff, K. Bange, and B. Hetz, *ibid.*, **135**, 1856 (1988).
13. G. Campet, B. Morel, M. Bourrel, J. M. Chabagno, D. Ferry, R. Garie, C. Quet, C. Geoffroy, J. J. Videau, J. Portier, C. Delmas, and J. Salardenne, *Mater. Sci. Eng.*, **138**, 303 (1991).
14. A. K. Sood, *J. Appl. Electrochem.*, **16**, 274 (1981).
15. M. Oshitani, T. Takayama, K. Takashima, and S. Tsuji, *This Journal*, **135**, 25 (1988).
16. W. H. Strehlow and E. L. Cook, *J. Phy. Chem. Ref. Data*, **2**, 163 (1973).

Electrode Properties of Sr-Doped $LaMnO_3$ on Yttria-Stabilized Zirconia

I. Three-Phase Boundary Area

F. H. van Heuveln,[a] H. J. M. Bouwmeester,[b] and F. P. F van Berkel[a]

[a]*Netherlands Energy Research Foundation ECN, 1755 ZG Petten, The Netherlands*
[b]*Department of Chemical Technology, Laboratory of Inorganic Materials Science, University of Twente, 7500 AE Enschede, The Netherlands*

ABSTRACT

The interface microstructure of the state-of-the-art cathode material for solid oxide fuel cells, $Sr_xLa_{1-x}MnO_3$ (SLM), was investigated with respect to its electrochemical performance. The interface microstructure was characterized by grain size and coverage of SLM on the electrolyte surface. Variation of the grain size was obtained by using three different sintering temperatures, whereas variation of the coverage was obtained by using two powders with a different morphology. This resulted in a set of six cathode/electrolyte samples with different combinations of grain size and SLM coverage at the interface. The cathode overpotential, as a measure for the electrochemical performance, could not be related to the length of the three-phase boundary. Based on the constriction resistance occurring in the electrolyte a model was developed which provides an estimate for the width of the active three-phase boundary zone.This zone is most likely to extend outside the cathode particle across the zirconia surface. The width calculated in this way was found to vary in the range of 0.03 to 0.07 μm for the different electrode microstructures. It is argued that the actual values may be smaller by one or two orders of magnitude.

Introduction

For solid oxide fuel cells (SOFCs) $Sr_xLa_{1-x}MnO_3$ is still the most widely used and favored cathode material. The performance of the SLM electrode is strongly determined by its interface microstructure.[1-3] Despite a lot of work carried out on SLM cathodes, there is not much knowledge available from the literature concerning (semi-) quantitative relations between the interface microstructure and electrochemical performance. A better understanding of this topic may lead to a useful tool for the optimization of SOFC cathode electrodes. Therefore, in this study a series of six different cathodes is investigated. The microstructure is varied by: (*i*) preparing cathodes from as-received powder and from the powder obtained after milling, and (*ii*) choosing three different sintering temperatures for cathodes prepared from both unmilled and milled powders. Particular attention is paid to the characterization of the microstructure at the interface in terms of particle contact diameter, total contact surface area between the SLM particles and yttria-stabilized zirconia (YSZ), and the three-phase boundary area (TPB). The relation between the microstructure and the electrode kinetics is the subject of Part II of this study.[4]

Experimental

Sample preparation.—Cathode powder was commercially obtained with composition $Sr_{0.15}La_{0.85}MnO_3$. The chemical composition of the SLM powders was checked by inductively coupled atomic emission spectroscopy (ICP-AES). X-ray diffraction was carried out to ensure the phase purity of the powder. A Guinier camera with Cu $K_{\alpha 1,2}$ radiation was used. To vary the microstructure the SLM powder batch was divided into two portions. One portion was attrition milled for 5 h, the other one remained unmilled. The particle size distribution of both powders was measured by a light scattering technique using a Malvern Mastersizer and vibrating the powders for 2 min in ethanol. Both powders were suspended into a binder system to make a suspension suitable for tape casting electrodes on presintered electrolyte plates. The electrolyte plates, disk-shaped 130 μm thick and 5.1 cm^2 surface area, consisted of 8 mole percent (m/o) yttria-stabilized zirconia (8YSZ, Tosoh Company). The electrode area of the working electrode was 3.0 cm^2. Electrode thicknesses were measured using an optical microscope and micrometer. To vary the particle size in the electrode, the electrodes were sintered at different temperatures, *i.e.*, 1100, 1200, and 1300°C. The resulting samples with corresponding labels are listed in Table I.

Structural characterization.—In order to facilitate semiquantitative calculations with regard to the interface microstructure, the mean particle size, mean contact area, and total contact surface area were determined from dif-

Table I. Cathode types, sintering temperatures,[a] and corresponding labels used in this report.

Cathode type	Sintering temperature (°C)	Label
$Sr_{0.15}La_{0.85}MnO_3$	1100	U-11[b]
	1200	U-12
	1300	U-13
$Sr_{0.15}La_{0.85}MnO_3$	1100	M-11[c]
	1200	M-12
	1300	M-13

[a]Sintering time 1 h.
[b]Cathodes prepared from unmilled powder.
[c]Cathodes prepared from milled powder.

ferent scanning electron microscopy (SEM) pictures. The mean particle size was determined by measuring the diameters of at least 100 grains. The contact area was determined by removing the top layer of the cathode. This procedure results in a "fingerprint" of the contact surface of the cathode particles on YSZ. An SEM picture was taken from this fingerprint and the contact area was analyzed by using tracing paper. The resulting contact area was determined by an image analysis program. An example of such a fingerprint, resulting after removing the cathode, is shown for the M-13 cathode in Fig. 1.

The chemical composition across the electrode/electrolyte interface was determined by a JEOL JXA-840 scanning electron microscope equipped with an energy dispersive x-ray spectrometer (EDX). For line scans across the SLM/YSZ interface, fracture surfaces of the samples were embedded in an araldit resin and carefully polished. A line scan across the electrode/electrolyte interface was made by measuring the x-ray counts of Sr (L-α), La (L-α), Mn (K-α), O (K-α), and Zr (L-α). Concentrations of these elements were determined at every 0.5 or 1 μm intervals by counting for 1 min per point. Five minutes per point were used for the La, Mn-analysis in YSZ in order to obtain a sufficiently high resolution.

Electrochemical characterization.—Impedance spectroscopy and *i-V* measurements were performed for characterizing the electrochemical properties of the cathode/electrolyte interface. Measurements were performed using a three-electrode setup as shown in Fig. 2, consisting of a working (SLM) and reference (SLM) electrode on one side and a platinum electrode as the counterelectrode on the other side of the electrolyte disk. The platinum electrode was deposited by a dc sputtering apparatus. The measurement setup consisted of a ceramic sample holder plus quartz tube, oven, mass flow controller, and a controlling unit. A Solartron Schlumberger frequency response analyzer (FRA) Model 1255 connected to a personal computer was used for impedance measurements. Analysis of the impedance data was done by nonlinear least squares fitting[5] of the impedance of an equivalent circuit to the experimental data.

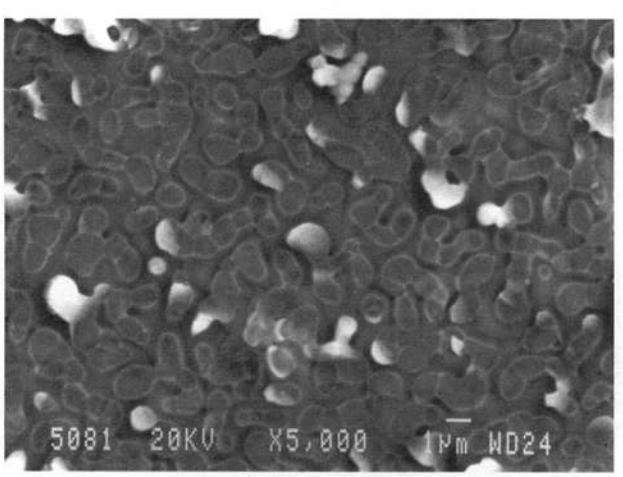

Fig. 1. Example of a fingerprint at the SLM/YSZ interface after removing the M-13 cathode microstructure from the YSZ substrate.

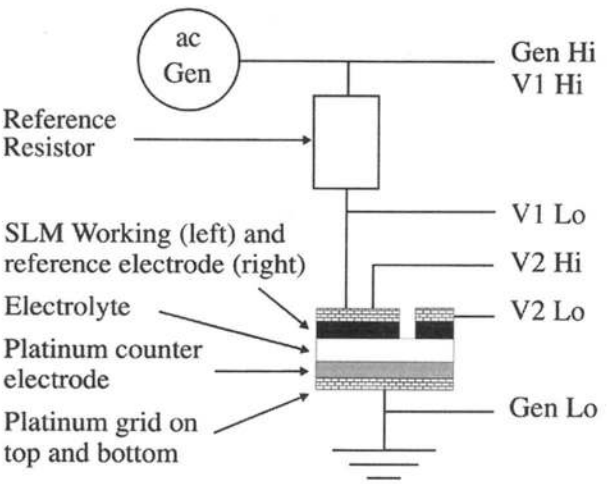

Fig. 2. Three-electrode setup with reference resistor for impedance measurements. Indicated are the positions of the analyzer channels V1 and V2 of the FRA. Hi and lo refer to the polarity of the analyzer channels.

As the high-frequency intercept plays an important role in characterizing the electrode/electrolyte interface (as discussed in the next section), the measurement setup was optimized with respect to high frequencies. Therefore no potentiostat was used and the sample leads were directly led to the FRA. To reduce influences of electromagnetic stray fields, a bifiliar-wound oven was used, a nickel shield was folded around the sample holder, and all measurement leads were kept as short as possible. A thermocouple was placed just beneath the sample. Fine mesh platinum grids were gently pressed on both sides of the sample. Measurements were carried out from 1 Hz to 1 MHz with 15 points per decade. A reference resistor in series with the sample was used to calculate the sample impedance. The reference resistor was adjusted in such a way that it was always larger than one tenth of the sample impedance, or smaller than ten times the sample impedance. The ac amplitude for the sample plus reference resistor was kept at 50 mV (peak-peak).

The sequence of performed measurements is schematically shown in Fig. 3. Using the electrode geometry as shown in Fig. 2, the measured electrode potential represents the total electrolyte loss, iR_o, including voltage loss due to the presence of a constriction resistance. This was demonstrated previously using different electrode geometries.[1] At 950°C a constant current of 100 mA/cm^2 was applied to the cathode/electrolyte samples for a period of 30 to 90 min. After the potential stabilized, the electrode potential was measured. Electrode overpotentials, η_{pol}, were calculated by subtracting the electrolyte loss, iR_o, from the measured electrode potential. For this correction the electrolyte resistance, R_o, was taken as the high-frequency intercept, R_{hf}, on the real-axis of the impedance diagram obtained immediately after the current polarization experiment. The resulting overpotential, η_{pol}, is considered as indicative for the electrochemical dc performance. Two minutes after switching off the current, the *i-V* characteristic and impedance were measured. The results of these measurements are presented in Part II of this study.[4]

Results

Chemical analysis of the SLM powders used showed a ratio of Sr:La:Mn = 0.152:0.842:1 with Mn normalized to 1. Cr, Ba, or Ca impurities were below the detection limit

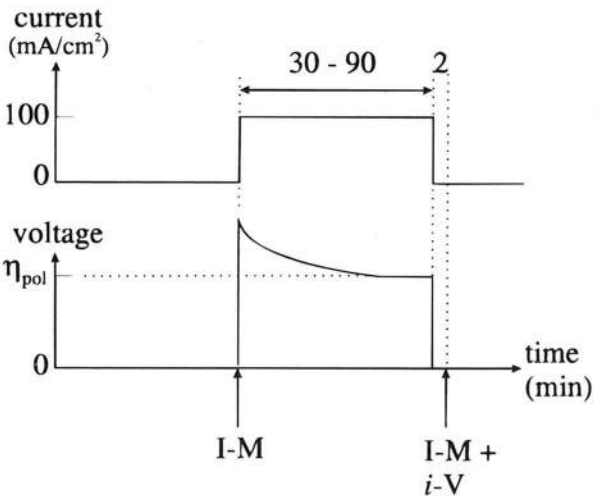

Fig. 3. Sketch of the measurement procedure. I-M refers to impedance measurement and *i-V* to the measurement of a current voltage characteristic. The resulting overpotential at the end of the current passage is denoted as η_{pol}.

(<0.005 w/o) of the ICP-AES technique. The powder was highly crystalline and showed a pure rhombhohedral phase. X-ray powder diffraction provided no evidence for other phases. Mean particle sizes determined from the particle size distribution (D_{50}) of the unmilled and milled powders are 5.5 and 1.4 μm, respectively.

Sample preparation.—SEM images taken from fracture surfaces of the different samples are given in Fig. 4. All cathodes showed adherence to the electrolyte.

Structural characterization.—Values for the mean particle diameter, d_g, the mean contact diameter, d_c, the total contact surface area, D_c, and the electrode thickness are given in Table II. Errors for d_g and d_c, given in Table II, are based on the determination of the area by the image analysis program and do not refer to the width of a distribution of these parameters. The parameters d_g and d_c with respect to an SLM particle at the YSZ surface are schematically

Table II. Measured values for the total contact surface area, D_c (relative to the geometrical electrode area), the electrolyte thickness, l, the electrode thickness, t, the mean grain diameter, d_g, and the mean particle contact diameter, d_c, of the SLM particle on YSZ.

Label	D_c (±10%) (%)	l (±5 μm) (μm)	t (±5 μm) (μm)	d_g (±15%) (μm)	d_c (±15%) (μm)
U-11	12	125	65	0.29	0.19
U-12	13.5	130	60	0.63	0.41
U-13	15	133	57	0.83	0.58
M-11	14	137	60	0.29	0.19
M-12	33	130	55	0.90	0.75
M-13	58	127	46	2.0	1.82

shown in Fig. 5. The mean particle diameter, d_g, and the mean contact diameter, d_c, are given in Fig. 6 as a function of sintering temperature. The contact surface area relative to the mean cross section of an SLM grain, expressed as $(d_c/d_g)^2$, is shown for different sintering temperatures in Fig. 7.

The three-phase boundary length (*TPBL*) per unit area of the electrode is defined as the total circumference, C, of N particles divided by the electrode geometrical area, and is given by

$$TPBL = \frac{C}{A_{geo}} = \frac{4D_c A_{geo}}{\pi d_c^2}\frac{\pi d_c}{A_{geo}} = \frac{4D_c}{d_c} \quad [1]$$

Note that in Eq. 1 D_c is expressed as fraction of the total electrode area, A_{geo}. Calculated *TPBL* values for the different cathode microstructures are given in Table III. Neither differences in the contact diameter, d_c, of the cathode particles at YSZ, nor other microstructural changes, were observed after the current passage. SEM images confirmed the contact area to be close to circular.

Concentration profiles from SEM-EDX line scan analysis for Sr, La, Mn, and Zr are shown for the M-11 cathode in Fig. 8 and for the M-13 cathode in Fig. 9. Concentrations are given as a function of the distance from the SLM/YSZ interface into the cathode. As can be seen from both figures, diffusion of zirconium occurs from the electrolyte into the cathode up to a distance of 4 μm from the interface. Moving away from the interface into the cathode bulk the zirconium concentration decreases and the

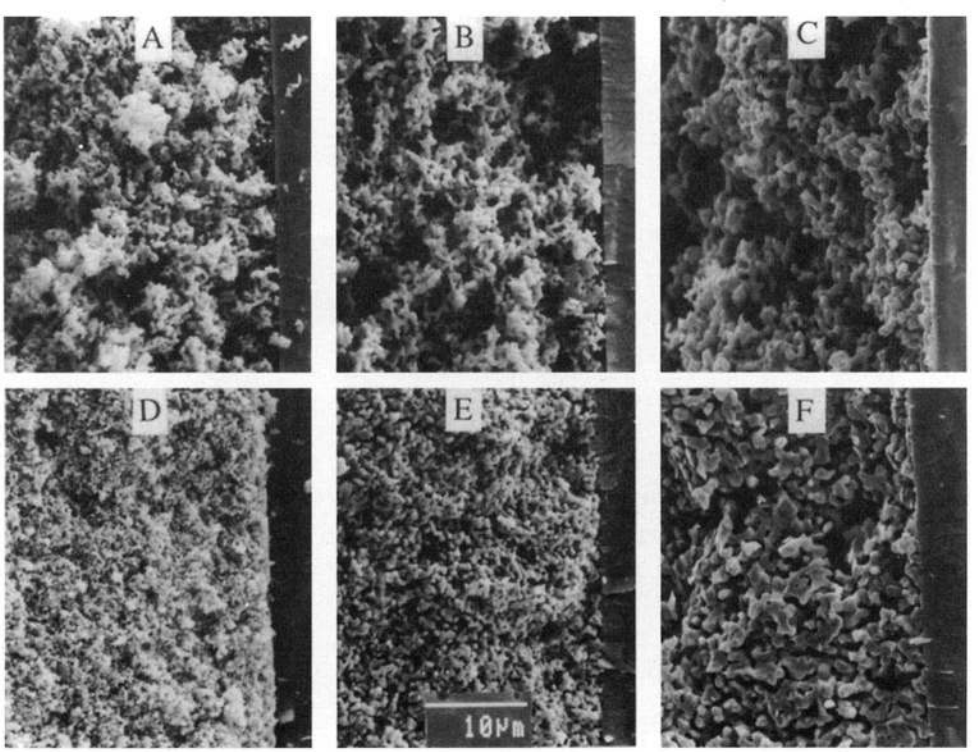

Fig. 4. Electron microscopy images of fracture surfaces from electrodes sintered at different temperatures (from left to right: 1100, 1200, and 1300°C) and prepared from SLM unmilled (A, B, and C) and milled (D, E, and F) powder. Part of the 8YSZ electrolyte can be seen at the far right side of the image. All images have the same magnification.

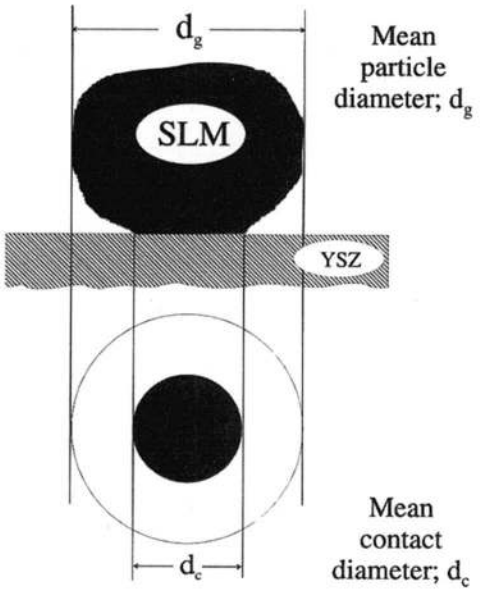

Fig. 5. Schematic representation of a cathode particle at the electrode/electrolyte interface. Important parameters are the mean grain diameter, d_g, and the mean contact diameter, d_c.

elemental distribution gradually reaches the "stoichiometric" composition of the SLM cathode. No yttrium could be detected in the cathode, which might partly be due to overlapping of EDX signals of Y and Zr. For the M-13 sample several contact points with the YSZ showed relatively high concentrations of Zr and decreased concentrations of Sr and Mn as compared to the cathode bulk composition. Diffusion of zirconium into the cathode material was also observed for the unmilled cathode series, although less pronounced as compared with the milled cathode series. Only for sintering temperatures of 1200°C or higher, for both the milled and unmilled series, Mn and La were found to diffuse from SLM into zirconia up to a distance of 2 μm from the interface.

Electrochemical characterization.—A model to obtain a semiquantitative measure for the active area of a porous-electrode/electrolyte interface has been presented in previous publications.[1,2] This model is based on the occurrence of constriction of the current lines in the electrolyte at the point where the current has to leave the electrolyte at the SLM/YSZ interface. The region where the current passes the interface is referred to as the three-phase boundary area. The loss in cross section for the current results in an increased electrolyte resistance. To treat experimental data of the electrolyte resistance, a simple measure for the electrolyte effective cross section, A_{cs}, was proposed[1,2]

$$A_{cs} = \frac{\rho_{ideal} l}{R_{hf}} \qquad [2]$$

in which ρ_{ideal} is the specific resistance of the electrolyte when no constriction is present (the value used is 0.07 Ω m, measured from an 8YSZ pellet with fine sputtered platinum electrodes), l the thickness of the electrolyte, and R_{hf} the high-frequency intercept at the real-axis of the impedance diagram. At the used temperature (945°C) the measured R_{hf} is considered equal to the electrolyte resistance. This means that other ohmic contributions arising from, *e.g.*, the contact between platinum grid and the cathode, or resistance due to a possible reaction layer, are considered not to contribute significantly to R_{hf}.

As all electrolytes were prepared in the same way and have comparable dimensions, the electrolyte resistance should be the same for all cathode/electrolyte structures. Using Eq. 2, A_{cs} can be calculated from the measured high-frequency intercept of the impedance spectra. Corresponding values were calculated after polarizing the sample and are given in Table IV. In this table A_{cs} is expressed

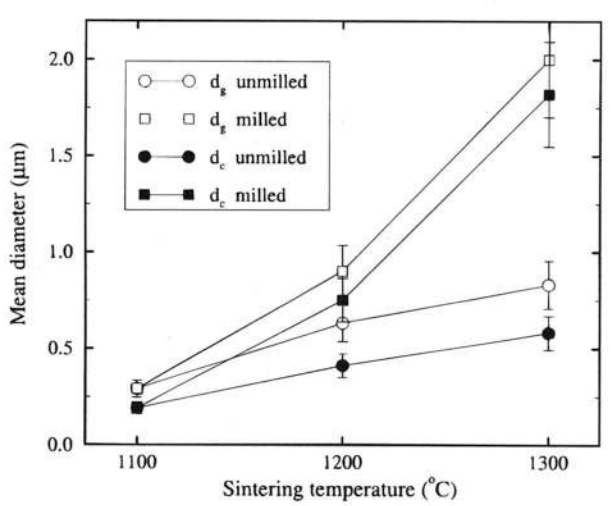

Fig. 6. Mean cathode particle diameter, d_g, (open symbols), and mean contact diameter d_c (filled symbols), for electrode microstructures prepared from SLM milled and unmilled powder on YSZ. Values are determined from SEM images.

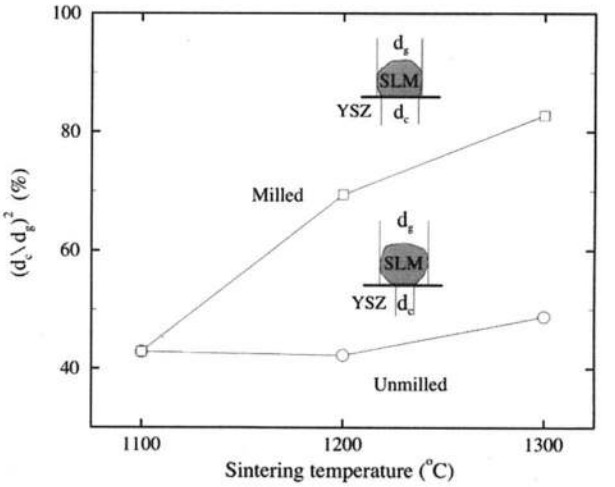

Fig. 7. Contact surface area at the electrode/electrolyte interfacerelative to the mean cross section of a cathode particle as a function of sintering temperature. The ratio of both areas is expressed as $(d_c/d_g)^2$.

Table III. Measured values for D_c and d_c (see also Table II) and calculated *TPBL* values for different SLM/YSZ interface microstructures.[a]

Label	Measured Dc (%)	Measured dc μm	Calculated *TPBL*[b] (cm/cm²)
U-11	12	0.19	2.54×10^4
U-12	13.5	0.41	1.32×10^4
U-13	15	0.58	1.03×10^4
M-11	14	0.19	2.97×10^4
M-12	33	0.75	1.77×10^4
M-13	58	1.82	1.27×10^4

[a]Measurments performed in air at T = 945°C.
[b]*TPBL* estimated error ±10%.

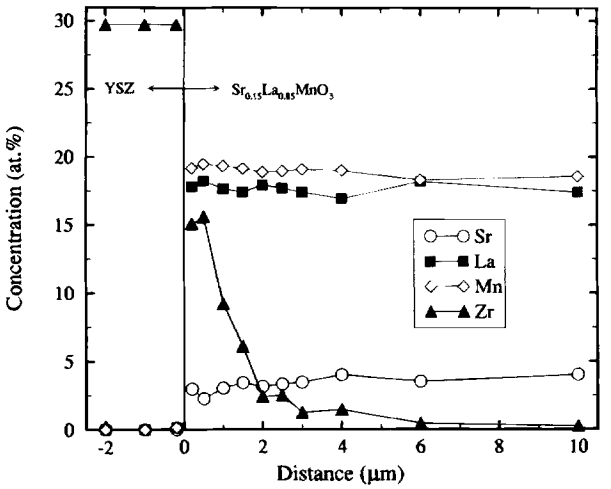

Fig. 8. Concentration profiles for La, Sr, Mn, and Zr as a function of the distance from the YSZ/SLM interface. Cathode is SLM sintered at 1100°C (M-11). Data was acquired by SEM-EDX on embedded fracture surfaces of SLM/YSZ interfaces.

as percentage of the geometrical electrode area A_{geo}. In the same table the high-frequency intercept R_{hf} is given. The cathode overpotentials, η_{pol}, corresponding to a constant current of 100 mA/cm^2 through the SLM/YSZ structures, are given also in Table IV. For all samples a steady-state situation was reached within less than 30 min. The voltage decreased strongly with time, just after switching on the current. For the milled cathodes the voltage may increase, as observed for the M-11 and M-13 cathodes.

Discussion

Structural characterization.—Milling removes many of the larger agglomerates, resulting in a more regular microstructure. Due to a high packing degree of submicron grains, a highly sinter-active electrode is formed. The high sinter activity of the milled cathode series is reflected in the sharp increase of the grain size with sintering temperature, as shown in Fig. 6. Consequently, larger particles achieve a larger contact area with YSZ, *i.e.*, a larger total contact surface area, D_c (see Table II). On the other hand, agglomerates in the unmilled cathode series reduce the sinter activity, resulting in smaller particles and consequently smaller D_c values. In this way a set of six cathode/electroyte interface microstructures with different

Table IV. Measured values for the overpotential, η_{pol}, the high-frequency intercept, R_{hf}, of the real-axis in the impedance diagram, and the calculated values for the electrolyte effective cross section, A_{cs},[a] for the different SLM/YSZ interface microstructures.[b]

Cathode label	Measured η_{pol} (mV)	Measured R_{hf} (Ω)	Calculated A_{cs} (%)
U-11	154	0.222	12.7 (5)
U-12	236	0.327	8.8 (7)
U-13	290	0.403	7.4 (4)
M-11	211	0.281	10.8 (12)
M-12	144	0.218	13.3 (3)
M-13	320	0.366	7.8 (4)

[a]Given as a percentage of the geomertric area, and the error given in parenthesis.
[b]Measurements performed in air at T = 945°C.

combinations of particle contact size and coverage was obtained.

From the literature it is well known that at the interface of zirconia with stoichiometric SLM having a low Sr content, lanthanum zirconate can be formed as a reaction product and, simultaneously, diffusion of Mn takes place into the electrolyte.[6,7] The amount of reaction products depends upon the sintering conditions and the microstructure of the SLM cathode. From the data shown in Fig. 8 and 9 it is anticipated that some lanthanum zirconate is formed at the interface. The less pronounced interdiffusion behavior at the SLM/YSZ interface of the unmilled cathodes is explained by less sinter activity of these cathodes as compared with the milled cathodes. Evidence for the occurrence of $SrZrO_3$ was not observed in this study, in accordance with other literature.[6,7] It is assumed that the observed interdiffusion does not contribute significantly to the ohmic losses.

TPB area and microstructure.—Cathodes prepared from unmilled powders lead to submicron particles at the interface and a low contact area of SLM on YSZ. Conversely, milling of the starting powder results in larger particles after sintering and a higher SLM contact area on YSZ. The TPBL values, calculated from Eq. 1, are plotted in Fig. 10 as a function of the cathode overpotential, η_{pol}. From this figure it can be seen that for all six cathodes, the TPBL values do not show a clear correlation with η_{pol}. A better correlation is found between the effective cross section, A_{cs}, determined from the measured high-frequency inter-

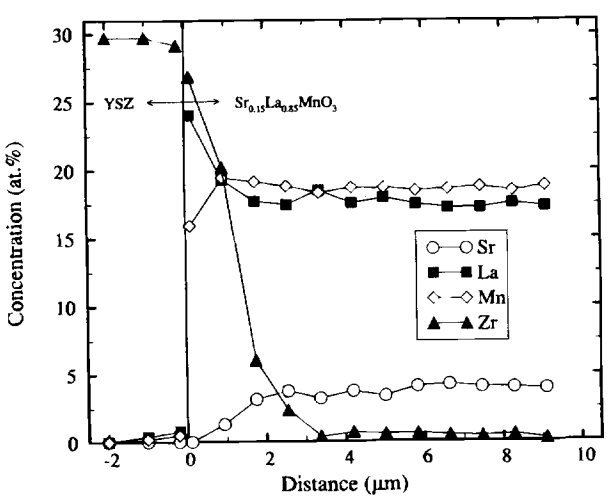

Fig. 9. Same as Fig. 8 but now for a cathode type sintered at 1300°C (M-13).

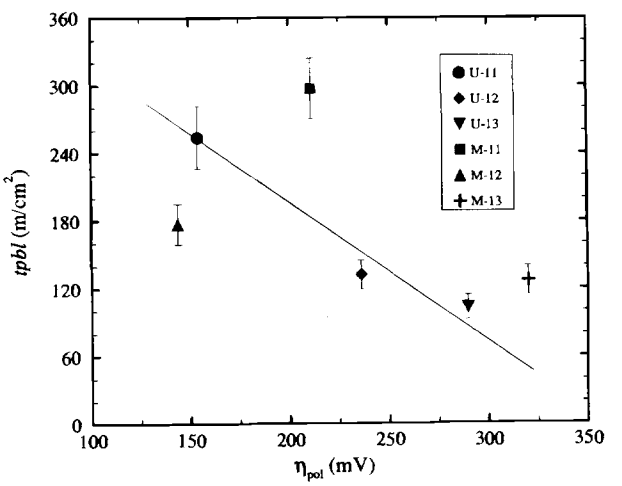

Fig. 10. Calculated *TPBL* values plotted as a function of the cathodic overpotential, η_{pol}, (i = 100 mA/cm^2) measured for different SLM/YSZ structures. Measurements were performed in air at T = 945°C.

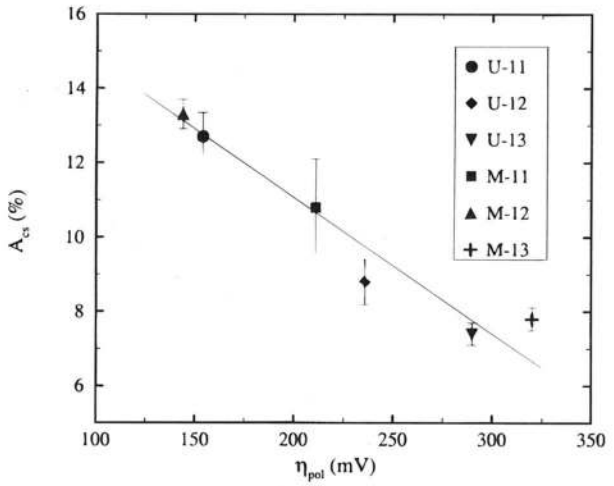

Fig. 11. The electrolyte cross-sectional area, A_{cs}, plotted as a function of the cathodic overpotential, η_{pol}, (i = 100 mA/cm^2) measured for different SLM/YSZ structures. Measurements were performed in air at T = 945°C.

cept resistance, R_{hf}, and η_{pol} for all six cathodes, as can be seen in Fig. 11. This observation suggests that A_{cs} is related to the TPB area or region at the electrode/electrolyte interface. Based upon a certain spatial extension of the TPB region, we need to consider only those regions that are able to affect the constriction resistance in the electrolyte. This means that we can restrict our analysis to a two-dimensional TPB area parallel to the YSZ surface. Two possible TPB areas, which extend parallel to the YSZ surface, are pathway 1, a zone outside the cathode particle at the electrolyte surface and pathway 2, a zone inside the cathode particle at the electrolyte surface. Both pathways are defined as a circular zone with a certain width, w, and an outer diameter. For pathway 1 the outer diameter of the TPB zone is $d_c + 2w$, and for pathway 2 it is d_c (see Fig. 12). Thus, if the width of the TPB zone is known its area can be calculated on the basis of the microstructural data, as given in Table II. The extension of the TPB zone into the cathode material (pathway 2) is considered to be less likely because of the small oxygen deficiency[8] and, hence, concomitant low rate of oxygen transport exhibited by SLM, even at reduced oxygen partial pressure. The oxygen partial pressure at the interface, corresponding with the highest observed overvoltage in our experiments, *i.e.*, 320 mV (*vs.* air) approximates 1×10^{-6} atm. At this oxygen partial pressure SLM exhibits near-ideal oxygen stoichiometry; thus, the ionic conductivity will be very low. It has been reported by Siebert *et al.*[9] that such a mechanism may become feasible at overpotentials in excess of 0.5 V (*vs.* air),[9] which corresponds to an oxygen partial pressure of 4×10^{-10} atm. However, pathway 2 cannot be excluded completely because of the possibility of enhanced oxygen transport via microcracks or grain boundaries.

The extension of the TPB zone outside the cathode particle (pathway 1) may be due to, *e.g.*, spillover of oxygen electroactive species, $O^-_{2,ad}$ or O^-_{ad}, across the zirconia surface. The corresponding effect on the constriction of the current lines in the electrolyte is schematically illustrated in Fig. 13. It should be noted that the extension of the TPB zone may also be influenced by the concentration of impurities or reaction products at the free electrolyte surface as a consequence of the processing procedure of the electrode/electrolyte structure.

Calculation of the width of the TPB zone.—Assuming a circular contact with diameter d_c at the electrolyte, the area of the TPB zone around a single particle is given by

$$A_p = \pi w(d_c \pm w) \quad [3]$$

in which w is the width of the TPB zone and + and − refer to the TPB zone outside (pathway 1) and inside the cathode particle (pathway 2), respectively. The TPB area relative to the particle contact area is then given by

$$A_p^{rel} = \frac{4w(d_c \pm w)}{d_c^2} \quad [4]$$

The number of particles, N, at the interface per unit area of the electrode can be calculated from the contact surface area, D_c, the geometrical electrode area, A_{geo}, and the mean contact diameter, d_c

$$N = \frac{4D_c A_{geo}}{\pi d_c^2} \quad [5]$$

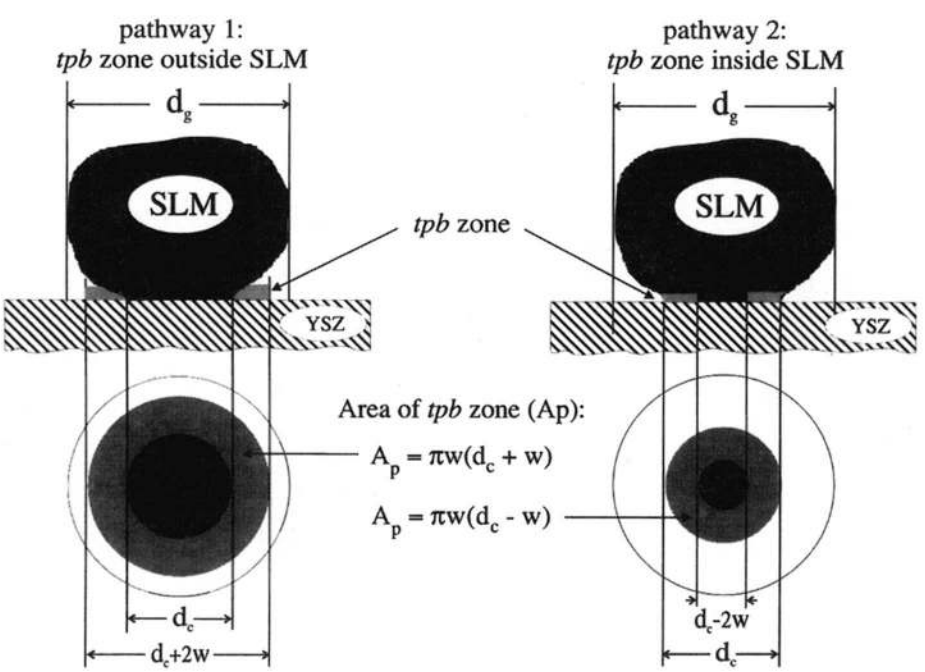

Fig. 12. Schematic representation of a cathode particle at the electrode/electrolyte interface. Left pathway 1 (TPB zone outside the cathode particle)and right pathway 2 (TPB zone inside the cathode particle).

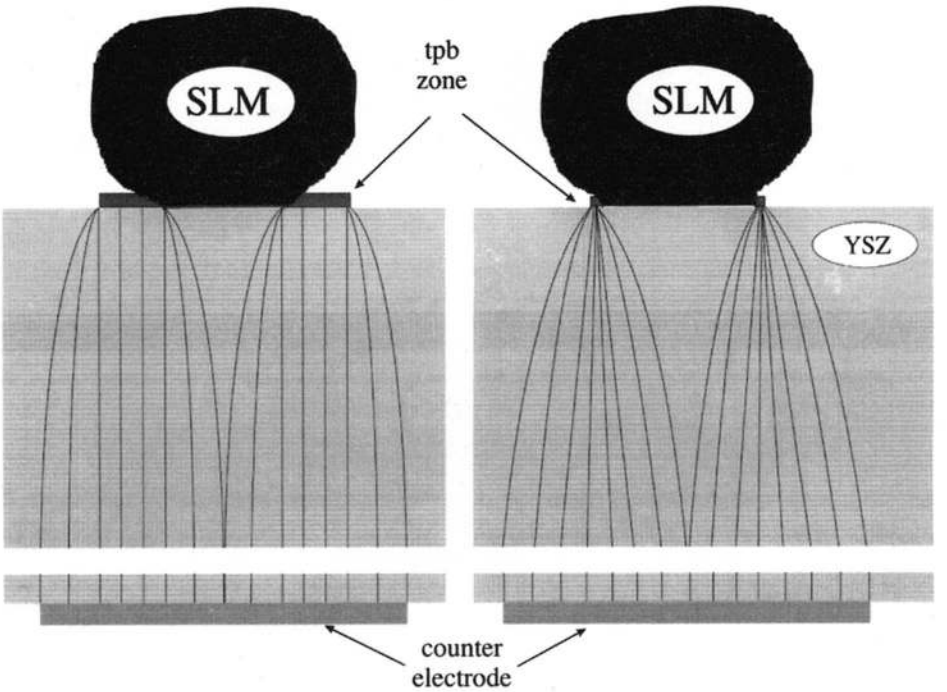

Fig. 13. Schematic representation showing the effect of a change in the width of the TPB zone on the constriction of the current lines in the electrolyte.

We now can calculate a total TPB area from the microstructure by multiplying the zone area of each particle, A_p, times N yielding

$$A_{tpb} = \frac{4D_c A_{geo}}{d_c^2} w(d_c \pm w) \quad [6]$$

w may be calculated through knowledge of A_{tpb}. The electrolyte effective cross section, A_{cs}, will be intermediate between A_{tpb} and A_{geo}. If we insert A_{cs} for A_{tpb} in Eq. 6, we may calculate an upper limit for w. Hence

$$\frac{4D_c A_{geo}}{d_c^2} w(d_c \pm w) = A_{cs} = \frac{\rho_{ideal} l}{R_{hf}} \quad [7]$$

which equation can be solved for pathway 1 into

$$w = \frac{-d_c}{2} + \frac{\sqrt{A_{geo} D_c R_{hf} d_c^2 (A_{geo} D_c R_{hf} + \rho_{ideal} l)}}{2A_{geo} D R_{hf}} \quad [8]$$

Using Eq. 8 values of w were calculated for every cathode microstructure. Corresponding values are given in Table V. Values for w are found between 0.03 and 0.07 μm, with a mean value of 0.05 ± 0.02 μm. Note that the calculated range of the w values is small, even though the particle size in the investigated electrodes differ by almost an order of magnitude, as shown in Table II. The total TPB area, at a given load, therefore increases with decreasing particle size.

By substituting the value of w back into Eq. 4, the TPB area as percentage of the contact area per cathode particle, A_p^{rel}, can be calculated. A_p^{rel} as a function of the mean contact diameter, d_c, is shown in Fig. 14. It is seen that for the cathodes sintered at 1100°C having the smallest particles, the TPB area is of the same order of magnitude as the contact area, *i.e.*, A_p^{rel} approximates 100%. For cathodes with larger grains and thus with larger contact areas, the TPB area (A_{cs}) is, at a given total SLM coverage, D_c, substantially reduced, cf. Tables II and IV.

The two parameters that determine the TPB area are d_c and D_c (see Eq. 6). When the TPB zone surrounds the cathode particle at the electrolyte surface, a large total TPB area, and thus a high electrochemical performance, is obtained when cathode particles are small and a high total coverage of SLM at the interface is achieved. This implies that a high particle loading is desired. These considerations hold for both pathways as long as $d_c > 2w$.

Table V. Calculated values for the width, *w*, of the TPB zone extending outside the cathode particle.[a]

Label	w[b] (μm)	Label	w (μm)
U-11	0.04	M-11	0.03
U-12	0.06	M-12	0.07
U-13	0.06	M-13	0.06

[a]Calculations refer to measurements in air at T = 945°C.
[b]Error ±15%.

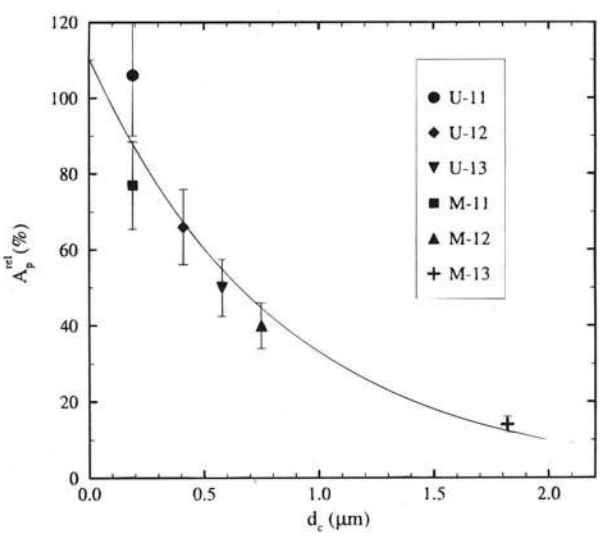

Fig. 14. The relative TPB area, A_p^{rel}, of a single cathode particle at the electrode/electrolyte interface plotted as a function of the mean contact diameter, d_c. Measurements were performed in air at T = 945°C. Solid line is a guide for the eye.

Values of w listed in Table V, are one to two orders of magnitude smaller compared with those reported by Kleitz *et al.*,[10] who calculated the TPB zone of Ag electrodes on YSZ to be around 1 μm. Based on the work of Mizusaki *et al.*,[11] Kleitz *et al.*[10] found a TPB zone for $La_{0.6}Ca_{0.4}MnO_3$ on a YSZ which would be significantly smaller than 1 μm.

As discussed previously, the occurrence of current constriction is attributed to the presence of discrete contact areas between the electrode and electrolyte. At these areas the current passes the interface. As shown by Tannenberger and Siegert,[12] the current in the electrolyte is already homogeneous above a distance from the interface that is of the order of the distance between the contact spots. Since in this study the electrolyte thickness is much larger than the distance between the electrode particles, the constriction effect would be confined to the immediate electrolyte surface, rather than extending across the entire thickness of the electrolyte. Consequently, the real TPB area will be smaller than A_{cs}, and hence, the actual values of w will be smaller than the calculated ones. It is estimated that the actual values may be smaller even by more than two orders of magnitude.

The present analysis may be complicated when the TPB area is coupled with reaction steps, *e.g.*, charge-transfer and surface diffusion of oxygen intermediate species occurring on the outer surface of the cathode particle. This is the main theme of Part II of this paper, the following article published in *This Journal*.[4]

Conclusions

By taking the sintering temperature and powder morphology as a variable it was possible to obtain a set of interface microstructures with varying values for the particle size at the interface and the total coverage of the cathode particles on the electrolyte surface.

The electrochemical performance of the investigated cathode/electrolyte structures can be related to the interface microstructure by extending the one-dimensional TPB line into a two-dimensional TPB zone. The analysis is based on the assumption that the constriction resistance of the electrolyte, derived from data of impedance measurements, is related to the effective TPB area. Combining the experimental value for this area (A_{cs}) with data obtained from the interface microstructure enables calculation of the extension of the TPB zone. Calculated widths of this zone for the different cathode/electrolyte structures were found to vary in the range 0.03 to 0.07 μm. It is argued that the actual values may be smaller by one or two orders of magnitude. Both the contact surface and total coverage of SLM particles at the interface determine the extension of the total TPB area. A high electrochemical performance is therefore obtained for a high particle loading at the cathode/electrolyte interface.

Acknowledgments

The authors acknowledge the contributions of R. Beenen for preparation of samples and measurements and G. Hamburg for the SEM and EDX work. This work was supported in part by the Commission of the European Communities in the framework of the JOULE program (Contract No. JOU2-CT92-0105).

Manuscript submitted April 25, 1996; revised manuscript received Sept. 11, 1996.

Netherlands Energy Research Foundation ECN assisted in meeting the publication costs of this article.

LIST OF SYMBOLS

A_{cs}	electrolyte effective cross-sectional area used as a relative measure for the TPB area
A_{geo}	geometrical electrode area
A_p^{el}	TPB area of a single cathode particle at the interface
A_p	relative to the particle contact area
d_c	mean contact diameter of a cathode particle at the interface
D_c	total contact surface area at the interface
d_g	mean diameter of a particle in the electrode
i	current density
l	thickness of the electrolyte
N	total number of particles at the electrode/electrolyte interface
R_{hf}	high frequency intercept on the real-axis in the impedance diagram
t	thickness of the electrode
w	width of the TPB zone

Greek

η	overpotential (after correction of iR drop)
η_{pol}	overpotential at the end of a constant current passage of 100 mA/cm^2 for 30 min
ρ_{ideal}	specific resistance of the electrolyte under ideal conditions, *i.e.*, no constriction of current lines

REFERENCES

1. F. H. Van Heuveln, F. P. F. Van Berkel, and J. P. P. Huijsmans, in *High Temperature Electrochemical Behavior of Fast Ion and Mixed Conductors, Proceedings of the 14th Risø International Symposium on Materials Science*, F. W. Poulsen, J. J. Bentzen, T. Jacobsen, E. Skou, and M. J. L. Østergärd, Editors, pp. 75-84, Risø National Laboratory, Roskilde, Denmark (1993).
2. F. P. F. Van Berkel, F. H. Van Heuveln, and J. P. P. Huijsmans, *Solid State Ionics*, **72**, 240 (1993).
3. K. Sasaki, J-P. Wurth, R. Gschwend, M. Gödickemeier, and L. J. Guackler, *This Journal*, **143**, 530 (1996).
4. F. H. van Heuveln and H. J. M. Bouwmeester, *This Journal*, **144**, 134 (1997).
5. B. A. Boukamp, EQUIVALENT CIRCUIT, A software program for ac immittance data analysis, Version 4.51, University of Twente, The Netherlands (1992).
6. J. A. M. van Roosmalen and E. H. P. Cordfunke, *Solid State Ionics*, **52**, 303 (1992).
7. H. Yokokawa, N. Sakai, T. Kawada, and M. Dokiya, *This Journal*, **138**, 2719 (1991).
8. J. H. Kuo, H. U. Anderson, and D. M. Sparlin, *J. Solid State Chem.*, **83**, 52 (1989).
9. E. Siebert, A. Hammouche, and M. Kleitz, *Electrochim. Acta*, **40**, 1741 (1995).
10. M. Kleitz, T. Kloidt, and L. Dessemond, in *High Temperature Electrochemical Behavior of Fast Ion and Mixed Conductors, Proceedings of the 14th Risø International Synposium on Materials Science*, F. W. Poulsen, J. J. Bentzen, T. Jacobsen, E. Skou, and M. J. L. Østergärd, Editors, pp. 89-116, Risø National Laboratory, Roskilde, Denmark (1993).
11. J. Mizusaki, H. Tagawa, K. Tsuneyoshi, and A. Sawata, *This Journal*, **138**, 1867 (1991).
12. H. Tannenberger and H. Siegert, *Adv. Chem.*, **90**, 281, Presented at the Chicago Meeting of the American Chemical Society, 1967 (1969).